

# Modulating the reactivity of Ni-containing Pt(111)-skin catalysts by density functional theory calculations

Hai-Yan Su,<sup>1,2,3</sup> Xin-He Bao,<sup>1,a)</sup> and Wei-Xue Li<sup>1,2,b)</sup>

<sup>1</sup>State Key Laboratory of Catalysis, Dalian Institute of Chemical Physics, Chinese Academy of Sciences, Dalian 116023, People's Republic of China

<sup>2</sup>Center for Theoretical and Computational Chemistry, Dalian Institute of Chemical Physics, Chinese Academy of Sciences, Dalian 116023, People's Republic of China

<sup>3</sup>Graduate School of the Chinese Academy of Sciences, Beijing 100039, People's Republic of China

(Received 19 December 2007; accepted 11 April 2008; published online 19 May 2008)

We present here a first principles density functional theory investigation of the reactivity of Pt(111)-skin catalysts, which are varied from surface alloys with Ni to bulk  $\text{Pt}_x\text{Ni}_{1-x}$  ( $x=0.25, 0.50, 0.75$ ) alloys. Molecule (CO, O, and H) adsorption and oxidation of CO+O and H+O reactions were studied and analyzed in detail. Independent of the adsorbates, the interaction between adsorbates and substrates becomes weakened with increase in Ni, due to the downshift of *d*-band center of surface Pt atoms. Moreover, activation barriers of CO and H oxidation toward atomic oxygen gradually decrease. In term of CO preferential oxidation (PROX) in excess of hydrogen, it turns out that the overall reactivity and selectivity rely on the optimum of various elementary steps involved such as competitive molecular (dissociative) adsorption and oxidation reaction. The present calculations show that  $\text{Pt}_3\text{Ni}$ (111) with Pt overlayer is an optimum catalyst for CO PROX in excess of hydrogen. © 2008 American Institute of Physics. [DOI: 10.1063/1.2920174]

## I. INTRODUCTION

Fundamental understanding and ability of control of molecules–transition metal (TM) interaction, as well as their dependence on structures and components, are the keys of catalysis, which play a crucial role in modern industries, energy, and environmental protections. A prominent example is low-temperature polymer electrolyte membrane fuel cells (PEMFCs), which convert chemical energy from fuel (hydrogen) to electricity with environmental friendly water as the only product. Among others, precious platinum are the most efficient, stable, and commercialized catalysts used at both anode and cathode to increase the reaction rates. Since hydrogen fuel normally comes from reforming process, the presence of a few percentage of carbon monoxide (CO) is inevitable and will eventually poison Pt catalysts. Improving Pt catalytic activity with better CO tolerance and decreasing amount of Pt, or even replacement of Pt, are the main challenges in the fields, which experimentally and theoretically attract extensive efforts.<sup>1–22</sup>

It has been found that the presence of the second elements, such as Ru, Sn, or Mo, by either alloying or codepositing with platinum was able to remarkably improve CO tolerance at anode.<sup>1–5</sup> The reason has been attributed to the variation of Pt electronic structures induced by alloying to destabilize CO–Pt bonds. Destabilization of spectators and intermediates (such as hydroxyl group) at cathode can also be realized by alloying to free moving active sites for oxygen reduction reaction (ORR).<sup>6–9</sup> Markovic and co-workers reported that bimetallic  $\text{Pt}_3\text{M}$  alloys ( $\text{M}=\text{Cr}, \text{Mn}, \text{Co}, \text{Ni}$ ) cata-

lysts dramatically enhanced the ORR reactivity.<sup>10,11</sup> Further characterization revealed that formation of the Pt overlayer (the so-called Pt skin) due to the segregation under operating conditions and decrease in lattice constant by alloying were the main driven forces behind not only for increasing number of active sites but also the activity of adsorbates.

CO poison can, however, be partially relieved by removing CO from reforming process via methanation, water gas shift reaction, and CO preferential oxidation (PROX).<sup>16–22</sup> Among them, CO PROX has merits of lower reaction temperature and high selectivity (decrease CO concentration to a few ppm) and received special attention. It has been found that supported PtSn alloy showed high activity and selectivity toward CO PROX in excess of hydrogen, where the turnover frequency was about two orders of magnitude higher on PtSn/C than that of the reference catalyst Pt/ $\text{Al}_2\text{O}_3$  at the fuel cell operating temperature of 80 °C.<sup>20,21</sup> Recently, Ko and co-workers reported that supported Pt–Ni and Pt–Co catalysts have high CO conversion and  $\text{CO}_2$  selectivity, where the presence of bimetallic Pt–Ni (Co) nanoparticles was found to be essential.<sup>22</sup>

Despite extensive efforts on CO PROX reaction carried out so far, microscopic understanding in terms of elementary reaction activity and selectivity as well as their dependence on the catalysts and stoichiometrics remained. To shed light on these, we report here a systematical density functional theory study of CO PROX on Ni-containing Pt-skin catalysts. The molecule (CO, H, and O) adsorption on Pt–Ni(111) alloys with different Ni concentrations has been studied, and elementary reactions of CO and H oxidation toward atomic oxygen have been calculated. It turns out that the overall reactivity and selectivity rely on the optimum of various elementary steps involved in competitive molecular

<sup>a)</sup>Electronic mail: xhbao@dicp.ac.cn.

<sup>b)</sup>Electronic mail: wxli@dicp.ac.cn.

(dissociative) adsorption and oxidation reaction. The present calculations show that Pt<sub>3</sub>Ni(111) with Pt overlayer is an optimum catalyst for CO PROX in excess of hydrogen.

## II. COMPUTATIONAL METHODS

The spin-polarized density functional theory (DFT) calculations were performed by using highly optimized DACAPO package,<sup>23</sup> where ultrasoft pseudopotentials were used to describe the ionic cores. The Kohn–Sham one-electron valence states were expanded in a plane-wave basis set with well converged kinetic cutoff at 340 eV. The exchange–correlation energy and potential were described by the generalized gradient functional, GGA-PW91.<sup>24</sup> During iterative diagonalization of the Kohn–Sham Hamiltonian, Fermi population of the Kohn–Sham states ( $k_B T = 0.1$  eV) and Pulay mixing of the resulting electronic density were used to improve the convergence, such that the total energy can be correspondingly extrapolated to absolute zero.

The Pt–Ni bimetallic surfaces were represented by four-layer slab separated by seven equivalent layers of vacuum. The top two layers of the slab and adsorbates were relaxed up to residual forces of less than 0.02 eV/Å, while the atoms in the bottom two layers were frozen in bulk-truncated positions. Supercells with (2×2) periodicity have been employed to simulate adsorption and reaction on the surfaces. Adsorbates were placed on one side of the slab, where a dipole correction has been applied to remove the artificial interaction by the presence of nonequivalent surfaces.<sup>25</sup> A Monkhorst Pack mesh with (4×4×1) grid was used for  $k$  points sampling in the surface Brillouin zone of the unit cells.

The calculated equilibrium lattice constants for bulk Pt (4.00 Å), Pt<sub>3</sub>Ni (3.90 Å), Pt<sub>2</sub>Ni<sub>2</sub> (3.87 Å), and PtNi<sub>3</sub> (3.67 Å), which are consistent with the previous experimental and DFT study,<sup>26–28</sup> have been used throughout the present work. Calculations for the isolated gas-phase molecules were carried out in a (12.0×12.1×12.2 Å<sup>3</sup>) unit cell and the Brillouin zone was sampled by single  $k$  point. The calculated gas-phase H<sub>2</sub> and O<sub>2</sub> bond energies are –4.56 and –5.57 eV, which agree well with experimental values –4.48 and –5.12 eV, respectively.<sup>29</sup>

The average adsorption energy ( $E_{\text{ads}}$ ) was calculated as  $E_{\text{ads}} = E_{\text{total}} - E_{\text{slab}} - E_{\text{molecule(g)}}$ , which is energy gain with respect to the adsorbates in the gas phase and the metal slab at infinite separation.  $E_{\text{total}}$ ,  $E_{\text{slab}}$ , and  $E_{\text{molecule(g)}}$  are the total energies of the relaxed adsorbate–substrate system, clean surface, and the molecules in the gas phase, respectively. Here, a negative (positive) value represents exothermic (endothermic) adsorption. Energy barriers were calculated by constrained bond lengths between reactants at various values separated by a step less than 0.1 Å with care being taken that the pathways (potential energy surfaces) become continuous.

## III. RESULTS

CO preferential oxidation in excess of hydrogen involves various processes, such as molecular adsorption/dissociation, CO and H oxidation, and desorption of products. High overall activity and selectivity sensitively depend

on balance and competition between these elementary processes. To address and optimize the reactivity of Pt catalysts, Pt(111) has been studied first. Pt(111) is an efficient oxidation catalyst due to its ability of dissociating O<sub>2</sub> at moderate temperature without bonding dissociated oxygen atom too strong. These can be justified from measured low dissociation temperature/barrier, ~150 K/0.29 eV,<sup>30</sup> and dissociation barriers of 0.37 eV (0.07 ML) and 0.52 eV (0.27 ML) from density functional theory calculations.<sup>31</sup> Calculated (dissociative) adsorption energies at 0.25 ML from present work are –1.04 eV/O (fcc), –1.65 eV/CO (atop), and –0.49 eV/H (fcc), which agree well with previous DFT and experimental studies.<sup>32–35</sup> For elementary oxidation of CO and H with atomic oxygen, calculated barriers are 0.74 and 0.86 eV, respectively, which are in good agreement with Refs. 36 and 37. From the preliminary data set, a strategy for designing new catalysts with improved reactivity can be visualized as follows. First, large CO adsorption energy (source of poison) indicates that there is a huge room available for destabilizing CO to increase the reactivity of CO oxidation for better selectivity/activity for CO PROX or CO tolerance at the anode. Since the destabilization will eventually equally applied on all reactants (for instance, H and O) and possible intermediates, significant weak H–Pt bonding will, however, set a severe limit for anode catalysts. For CO PROX catalysts, a large drop of adsorption energy may efficiently prevent O<sub>2</sub> dissociation, which will lower the overall reactivity. An optimum between these processes is, therefore, required. Finally, we note that the barrier for CO oxidation is lower than that of H oxidation, which indicates intrinsic preferential selectivity of CO oxidation on Pt(111) than that of H.

To utilize the features of Pt(111) surfaces and improve reactivity and selectivity further, developing catalysts with Pt skin modified by second components underneath may be alternative. Indeed, catalysts with Pt skin have been found to have superior reactivity at various reactions, where acid and reducing conditions were applied.<sup>10,38,39</sup> Under these conditions, the formation of Pt-skin catalysts via Pt segregation from the subsurface to the surface was essential and well characterized by various experimental techniques<sup>10</sup> and theoretical calculations.<sup>40,41</sup> The driven forces behind were the lower surface energy and large atomic size of Pt than those of alloyed 3d transition metals. The preference of Pt skin is, however, true not only for bulk alloys but also for surface alloys. To justify this, a seven-layer Pt(111) slab with (2×2) periodicity has been constructed, where a quarter monolayer of Pt has been substituted at various places from top-most Pt layer to middle Pt layer of the slab. It was found that occupation of Ni at the subsurface region right below surface Pt layer is energetically the most favorable, which are 0.42 and 0.04 eV lower than that of substitution at the surface Pt layer and deeper in bulk, respectively. If placing one more Ni atom (with overall coverage of 0.50 ML) in Pt lattice, the calculations show that added Ni atom prefers to occupy the same subsurface layer, instead of going into the bulk, whose total energy is 0.12 eV higher.

Above discussion indicates that Pt-skin catalysts are energetically favorable for both surface and bulk alloys. Based on this, various Ni-containing Pt-skin (111) surfaces with

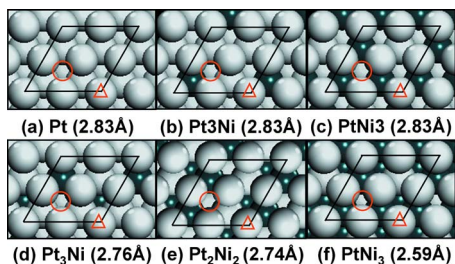


FIG. 1. (Color online) Schematic structures (top view) of Pt-skin (111) surfaces with different amounts of Ni from pure Pt (a), subsurface Pt<sub>3</sub>Ni (b), and PtNi<sub>3</sub> (c), to bulk Pt–Ni alloys Pt<sub>3</sub>Ni (d), Pt<sub>2</sub>Ni<sub>2</sub> (e), and PtNi<sub>3</sub> (f). The optimized lateral constants are given in brackets. The white and dark green spheres represent Pt and Ni atoms, and favorable adsorption sites are indicated by circles (for O and H) and triangle (CO), respectively.

(2 × 2) periodicity with different concentrations of Ni for surface alloy and lattice constants for bulk alloy have been set up and shown schematically in Fig. 1. Compared to pure Pt(111) [Fig. 1(a)], Figs. 1(b) and 1(c) represent surfaces with one (noted as Pt<sub>3</sub>Ni) and three quarter (PtNi<sub>3</sub>) Pt atoms in the second Pt layer substituted by Ni atoms. Since Pt<sub>3</sub>Ni and PtNi<sub>3</sub> surfaces have the exact same lateral lattice constants of Pt(111), the effect on the reactivity induced by Ni will come from ligand effect. Increasing Ni concentration further, three Pt<sub>x</sub>Ni<sub>1-x</sub> ( $x=0.25, 0.50, 0.75$ ) bulk alloys with Pt skin were considered, and the structures are schematically plotted in Fig. 1(d) for Pt<sub>3</sub>Ni (L<sub>12</sub>), Fig. 1(e) for Pt<sub>2</sub>Ni<sub>2</sub> (L<sub>10</sub>), and Fig. 1(f) for PtNi<sub>3</sub> (L<sub>12</sub>). Compared to the lattice constant of Pt 4.00 Å, lattice constant of three alloys gradually decreases from 3.90, 3.87, to 3.67 Å, respectively. Concerning Pt<sub>3</sub>Ni (b) and Pt<sub>3</sub>Ni (d) surfaces, we note that both surfaces share the same local stoichiometries within top two layers, and the ligand effect is roughly the same for both surfaces. The difference in lattice constants between two surfaces introduces additional strain effect in bulk alloys. The same applies to PtNi<sub>3</sub> (c) and PtNi<sub>3</sub> (f) surfaces, in which the ligand effect is enhanced further due to increase in the amount of Ni, compared to Pt<sub>3</sub>Ni (b) and (d), respectively.

As discussed above, although above setup exposes the same Pt-covered surfaces, they are different in terms of the amount of Ni underneath and lateral lattice constants. Exposed surface Pt layer may have distinct electronic properties, which will affect the reactivity, correspondingly. The variation of the electronic properties of surface Pt layer among these surfaces can be seen from projected *d*-band density of states (DOS) of surface Pt atoms, which are plotted in Fig. 2. It was found that with the increase in content of Ni from surface alloys [(b) and (c)] to bulk alloys [(d), (e) and (f)], the overall DOS and *d*-band center  $\epsilon_d$  continuously shift downwards from Fermi level, and DOS at Fermi level decreases, accordingly. It has been well established that these variations have significant effect on the surface reactivity; specifically, the downshift of *d*-band centers tends to weaken the interaction between reactants and substrates.<sup>42</sup> A consequence of weakened interaction between reactants and substrates may lead to dissociation thermodynamically less driven and raise the barrier of the dissociation. On the other hand, the destabilization may, however, promote recombina-

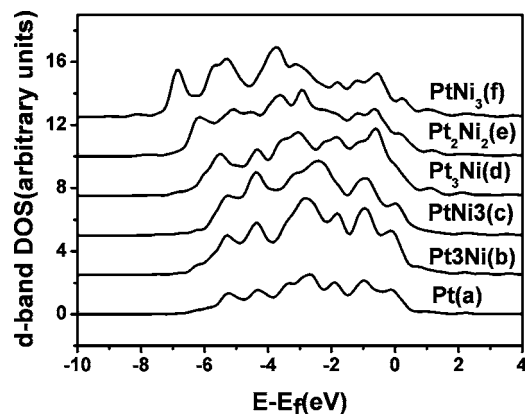


FIG. 2. Projected *d*-band DOS of surface Pt atoms coordinated with adsorbates of different Pt–Ni surfaces. The energy reference is the Fermi level.

tion reactions on the surfaces and facilitate desorption from the surfaces, as will be seen at the following discussion.

The effect of alloys on the reactivity has been studied by adsorption of CO, O, and H on different surfaces. In this context, various adsorption sites were considered. For simplicity, only the results for adsorption of CO at atop sites, and O and H at fcc hollow sites, as indicated in Fig. 1, were discussed in the present. Calculated adsorption energies are shown in Fig. 3 and listed in Table I, where different surfaces are represented by single parameter, averaged  $\epsilon_d$  of surface Pt atoms coordinated with the adsorbates. Independent of the reactants, it is found that adsorption energy  $E_{\text{ads}}$  decreases with position of  $\epsilon_d$ . Moreover, there is a linear relationship between  $E_{\text{ads}}$  and  $\epsilon_d$  found. Since position of  $\epsilon_d$  is proportional to the amount of Ni (Fig. 2), present results show that the bonding between reactants and substrates becomes weak with increase in amount of Ni. From the right to the left, the first three points correspond to the molecular adsorption on Pt (a), Pt<sub>3</sub>Ni (b), and PtNi<sub>3</sub> (c) surfaces, where the ligand effect from subsurface Ni for latter two surfaces are introduced and sequentially increases. Correspondingly, adsorption energies decreases by 0.14 eV (CO), 0.15 eV (O), and 0.16 eV (H). If one proceeds to the left further to Pt<sub>3</sub>Ni (d), Pt<sub>2</sub>Ni<sub>2</sub> (e), and PtNi<sub>3</sub> (f) surfaces with smaller lattice constants, additional strain effect [compared to Pt<sub>3</sub>Ni (b) and PtNi<sub>3</sub> (c) surfaces] are included. These result in a further

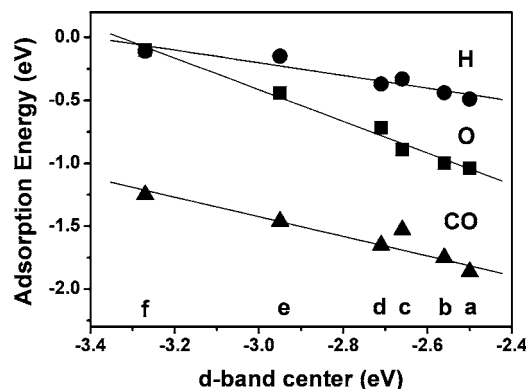


FIG. 3. Calculated adsorption energies  $E_{\text{ads}}$  for CO (triangle), O (square), and H (circle) vs the center of *d*-band on different surfaces, as defined in Fig. 1.

TABLE I. Calculated adsorption energies ( $E_{\text{ads}}$  in eV) and adsorption sites of the CO, O, and H at a coverage of 1/4 ML on different PtNi surfaces.

Surface	CO		O		H	
	$E_{\text{ads}}$	Site	$E_{\text{ads}}$	Site	$E_{\text{ads}}$	Site
PtNi <sub>3</sub>	-1.19	top	-0.1	fcc	-0.11	fcc
Pt <sub>2</sub> Ni <sub>2</sub>	-1.28	top	-0.44	fcc	-0.15	fcc
Pt <sub>3</sub> Ni	-1.53	top	-0.72	fcc	-0.37	fcc
PtNi <sub>3</sub>	-1.51	top	-0.89	fcc	-0.33	fcc
Pt <sub>3</sub> Ni	-1.68	top	-1.00	fcc	-0.44	fcc
Pt	-1.65	top	-1.04	fcc	-0.49	fcc

decrease in adsorption energies on Pt<sub>3</sub>Ni (d) and PtNi<sub>3</sub> (f) surfaces by 0.34 eV for CO, 0.62 eV for O, and 0.26 eV for H, respectively. From these analyses, it is clear that there is a huge space available to adjust adsorbate-Pt bond strength through alloying, which can be used to tailor the reactivity of catalytic reactions.

Having studied the effect of alloying on adsorption, we now turn to investigate its effects on the elementary reactions of CO and H oxidation with atomic oxygen within (2×2) supercells, where various coadsorption patterns have been considered. In given (2×2) cells, it is found that energetically most favorable coadsorption structures share a common pattern: oxygen adsorb at fcc hollow sites (circle indicated in Fig. 1) and CO and H at the top sites (triangle in Fig. 1) on different Pt–Ni surfaces except for PtNi<sub>3</sub>, where H prefers to adsorb at fcc hollow sites. The coadsorption patterns identified were used as the initial states (ISs) for following studies of the transition states (TSSs). Calculated barriers  $E_{\text{act}}$  for CO and H oxidation versus O adsorption energy  $E_{\text{ads}}$  are plotted in Fig. 4 and given in Table II. It is found that for both reactions,  $E_{\text{act}}$  decreases with  $E_{\text{ads}}$ . Furthermore, there is a linear correlation between  $E_{\text{act}}$  and  $E_{\text{ads}}$ . The reason behind and its implication will be discussed later. It is noted that although the TSSs were calculated in comparably small (2×2) cell, where lateral interaction between reactants may affect absolute value of activation energies, it may have a little effect on the trend identified here. This is because the same supercells have been used in these calculations, and the lateral interaction if any would be largely cancelled out.

As shown in Fig. 4, Pt<sub>2</sub>Ni<sub>2</sub> (e) and PtNi<sub>3</sub> (f) surfaces are

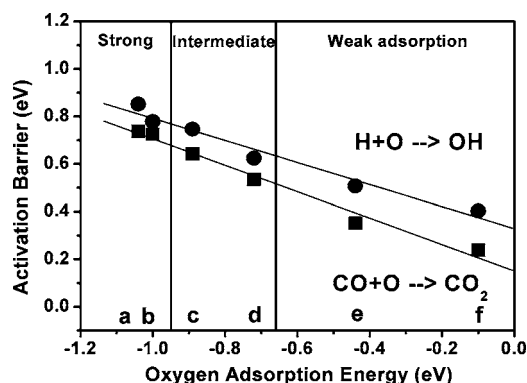


FIG. 4. Calculated activation barriers  $E_{\text{act}}$  for CO (square) and H (circle) oxidation vs oxygen adsorption energy on different surfaces, as defined in Fig. 1.

highly reactive with very low activation barriers for CO oxidation, 0.35 and 0.24 eV, stark contrast to Pt(111) 0.74 eV. Despite high reactivity of elementary oxidation, we note that dissociative O adsorption energies on two surfaces, -0.44 eV for Pt<sub>2</sub>Ni<sub>2</sub> and -0.10 eV for PtNi<sub>3</sub>, are significantly weaker than that of Pt(111) (-1.04 eV). As mentioned earlier, oxygen (dissociative) adsorption requires activation [barrier of ~0.71 eV in (2×2) cell]. According to Sabatier principle,<sup>43</sup> decrease in (dissociative) adsorption energy of oxygen will proportionally raise the dissociation barrier of oxygen molecules. Significant drop of adsorption energy on Pt<sub>2</sub>Ni<sub>2</sub> and PtNi<sub>3</sub> surfaces indicates large increase in the dissociation barrier. These will lower the overall activity for CO oxidation. For H oxidation, there is additional concern with respect to efficient H adsorption. As shown in Table I, calculated adsorption energies of hydrogen are -0.26 eV/H for Pt<sub>2</sub>Ni<sub>2</sub> and -0.11 eV/H for PtNi<sub>3</sub> (no zero vibration included), respectively. Although the weak adsorption is preferred for CO PROX in the case of Langmuir–Hinshelwood mechanism, it may not be good for electrochemical reaction at the anode, where efficient H adsorption is crucial. These analyses suggest that despite Pt<sub>2</sub>Ni<sub>2</sub> and PtNi<sub>3</sub> are highly reactive in terms of elementary oxidation reactions and contain much less amount of the Pt, which is cost competitive, poor overall reactivity makes them less promising.

For Pt<sub>3</sub>Ni (d) surfaces, calculated barriers for CO and H oxidation are 0.54 and 0.62 eV, in contrast to 0.74 and 0.86 eV on Pt(111), respectively. Pronounced improvement of reactivity of elementary reactions compared to Pt(111) can be seen. Meanwhile, the variation of corresponding O–Pt bond strength, -0.72 eV, compared to -1.04 eV on Pt(111), is modest, which indicates that O<sub>2</sub> dissociation remained efficient on Pt<sub>3</sub>Ni. This was supported further by explicit calculation of the TS with a barrier of 0.97 eV, which is just

TABLE II. Calculated activation energies ( $E_{\text{act}}$  in eV) for CO+O and H+O oxidation on different PtNi surfaces with (2×2) unit cells.

Surface	CO+O	H+O
PtNi <sub>3</sub>	0.24	0.4
Pt <sub>2</sub> Ni <sub>2</sub>	0.35	0.51
Pt <sub>3</sub> Ni	0.54	0.62
PtNi <sub>3</sub>	0.64	0.75
Pt <sub>3</sub> Ni	0.73	0.78
Pt	0.74	0.86

0.26 eV higher than that of Pt(111). The calculated barrier of O<sub>2</sub> dissociation on Pt<sub>3</sub>Ni is higher than CO oxidation (0.74 eV) on Pt(111), which apparently makes Pt<sub>3</sub>Ni less efficient than Pt alone. We note that this comes from artificial effect of limited (2×2) supercell used. As mentioned earlier, O<sub>2</sub> dissociation on Pt(111) is coverage dependent<sup>31</sup> and decreases with coverage. It is expected that this applies on Pt<sub>3</sub>Ni surfaces as well. This is particularly true in reality, where relative lower oxygen partial pressures were applied for CO PROX in excess of hydrogen. On the other hand, the relative activity of CO oxidation among different Pt–Ni surfaces is less affected since the same supercells have been applied on different surfaces. Hydrogen adsorption energy of –0.37 eV is reasonably stronger than those of Pt<sub>2</sub>Ni<sub>2</sub> and PtNi<sub>3</sub>, which indicates that Pt<sub>3</sub>Ni may be a potential catalyst used at anode. For CO PROX in excess of hydrogen, weakened interaction between H and catalysts is preferential for the selectivity of CO oxidation. We, therefore, conclude that high overall reactivity was reached on Pt<sub>3</sub>Ni surfaces.

For Pt<sub>3</sub>Ni (b) and PtNi<sub>3</sub> (c), where one and three quarters of subsurface Pt atoms were substituted by Ni atoms, calculated barriers are 0.73 and 0.64 eV for CO oxidation and 0.78 and 0.75 eV for H oxidation, correspondingly. Although these two surfaces may not suffer the difficulty of O<sub>2</sub> dissociation, the modest improvement of overall reactivity compared to Pt(111) makes them, however, less efficient than Pt<sub>3</sub>Ni.

#### IV. DISCUSSIONS

Above calculations indicate that Ni-containing Pt-skin catalysts are thermodynamically stable structures, particularly for the reaction under reducing conditions. Surface reactivity can be dramatically changed by alloying, and adsorption energies and reaction barriers can vary as large as ~1.00 and ~0.5 eV, respectively. When Ni concentration is low, Ni atoms prefer to occupy at the subsurface region right below surface layer and form surface alloys (Pt<sub>3</sub>Ni and PtNi<sub>3</sub> in present case). The modification on the reactivity from ligand effect is modest. With increase in Ni concentration further, Ni atoms start to incorporate into the bulk, and bulk alloys with shrinking of lattice constants (Pt<sub>3</sub>Ni, Pt<sub>2</sub>Ni<sub>2</sub>, and PtNi<sub>3</sub>) are developed. Besides the ligand effect induced by subsurface Ni, shrinking of lattice constants of bulk alloy introduces additional strain, which results in a significant variation of reactivity. The different surfaces can be characterized by a single parameter, which is center of *d*-band of surface Pt atom and gradually downshifts from Fermi level with increase in amount of Ni atoms. A linear relationship between *d*-band centers and adsorption energies of various molecules as well as reaction barriers shows intrinsic correlation between structure and reactivity, which will be discussed below.

The finding of linear relationship between *d*-band centers and adsorption energies has been well understood<sup>42</sup> and will not be addressed further. Instead, linear correlation between oxidation (CO and H) barriers and oxygen adsorption energies identified was discussed. To do so, we studied the geometries of TSs on different surfaces. Common features at

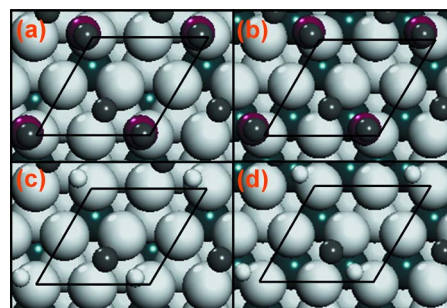


FIG. 5. (Color online) Calculated structures (top views) at TSs for CO oxidation on Pt<sub>3</sub>Ni(111) (a) and PtNi<sub>3</sub>(111) (b), and H oxidation on Pt<sub>3</sub>Ni(111) (c) and PtNi<sub>3</sub>(111) (d). The large white and dark green spheres represent for Pt and Ni atoms, while small white, middle purple, and gray spheres represent for H, C, and O, respectively.

TSs were found: O is activated from hollow sites to bridge sites and CO/H is off the top site. As representative examples, the TSs on Pt<sub>3</sub>Ni and PtNi<sub>3</sub> surfaces are schematically shown in Fig. 5. The similarity at TSs indicates that the difference between reaction barriers is mainly determined by the difference between adsorption energies of reactants at ISs, as found from Fig. 3. The weaker adsorption energies are, the smaller activations required are. Further insights can be found from dependence of bond lengths between reactants at TSs on different surfaces, as plotted in Fig. 6. For both CO and H oxidations, the activation barriers decrease with increase in bond length between reactants (OC–O and O–H) at TSs, and the reason behind is evident. For recombination reactions on surfaces, reactant-metal bond breaking and reactant-oxidant bond forming are involved, and the balance between them met at TSs determines the magnitude of reaction barriers. If the interaction between reactants and metal substrates is strong, the process of bond breaking is demanding. Reactants have to come closer to compensate the cost for bond breaking, and the reaction barrier is higher, correspondingly. We note here that the similar relationship between reaction barriers and chemisorption energies of reactants has been previously reported by Liu and Hu.<sup>44</sup>

Present calculations (cf. Fig. 4) showed that the barrier of CO oxidation is lower than that of H oxidation on Pt(111). This comes from the fact that smooth potential energy sur-

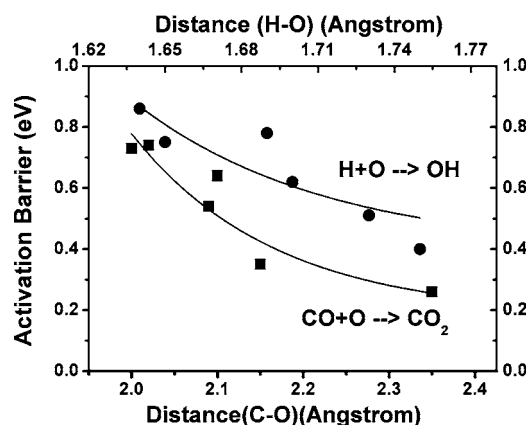


FIG. 6. Dependence of the calculated activation energies (in eV) for CO (square) and H (circle) oxidation on the bond length between reactants at TSs (in Å).

face of CO on Pt(111), and CO activation is less demanding. Furthermore, the preference of CO oxidation over H oxidation has been found for all Pt-skin catalysts considered, which indicates that all of the Pt-skin catalysts considered are potential catalysts for CO PROX reaction. The reason for this may come from the similar coadsorption pattern of reactants and TS on different Pt-skin catalysts, as shown above. Although absolute activity may vary on different alloys, it has a little effect on their relative difference. From Fig. 4, it is clear that Pt<sub>2</sub>Ni<sub>2</sub> and PtNi<sub>3</sub> have very low oxidation barrier, which is good in terms of elementary reactivity. On the other hand, poor oxygen dissociation and adsorption may, however, limit the overall reactivity and is, therefore, undesired. What is more important is that the barriers for both CO and H oxidations on two surfaces are so low that both reactions are highly reactive, which will result in low CO<sub>2</sub> selectivity. For Pt<sub>3</sub>Ni and PtNi<sub>3</sub> (surface alloy), we note that the improvement of reactivity is modest. Based on these, we concluded that Pt<sub>3</sub>Ni with Pt skin is an optimum catalyst for CO PROX reaction in excess hydrogen.

Above analyses are in line with recent experimental results of CO PROX on Pt–Ni catalysts supported on  $\gamma$ -Al<sub>2</sub>O<sub>3</sub>, which are reported by Ko *et al.*,<sup>22</sup> where superior reactivity and selectivity of bimetallic Pt–Ni particles compared to that of Pt were found. Compared to Pt alone, amount of CO chemisorption on bimetallic Pt–Ni catalysts was found to decrease, which can be understood from weakened CO–Pt interaction from the present calculations. Transmission electron microscopy and energy dispersive x-ray spectroscopy measurements showed that atomic ratio of Ni/Pt in bimetallic phase was larger than 0.5, which suggests formation of Pt–Ni bulk alloys. To reduce the samples at high temperature (773 K), bimetallic Pt–Ni phase was Ni enriched further, and CO selectivity decreased. These experimental findings nicely agree with the scenario from above theoretical calculations, which suggest that Pt<sub>3</sub>Ni could be the active phase for CO PROX in excess of hydrogen in experiment.

Pt–M catalysts with Pt overlayer may have wide implications on different catalytic reactions under reducing conditions. Indeed, its application has already been illustrated in the cathode ORR of PEMFC,<sup>10</sup> where Pt<sub>3</sub>M type of alloys with Pt skin are found to be highly active than that of pure Pt catalysts. Moreover, Pt(111) surfaces with the second TMs at the subsurface region have been recently demonstrated to improve the reactivity of water gas shift reaction<sup>38</sup> and the selective hydrogenation of C=O bond in acrolein.<sup>39</sup> We expect that there are even more remained to be explored.

## V. CONCLUSIONS

By systematic DFT calculations, we show that the catalytic activity and selectivity of Pt–M(111) alloys (Ni in the present case) with Pt overlayer can be efficiently modulated by doping various amount of TMs. Depending on the amount of added TMs, different surface alloys and bulk alloys with distinct electronic properties and reactivity formed, and inherent relationship between structure and activity was established. It was found that variation of electronic properties (downshift of *d*-band center of surface Pt atoms) was domi-

nated by the ligand effect for surface alloys, while dominated by both ligand and strain effects for bulk alloys. Concerning molecule (CO, H, and O) adsorptions, linear relationship between *d*-band centers, adsorption energies, and elementary reaction barriers (CO and H oxidation) has been found. In terms of CO PROX in excess of hydrogen, it turns out that the overall reactivity and selectivity rely on the optimum of various elementary steps involved in competitive molecular (dissociative) adsorption and oxidation reaction. Present calculations show that Pt<sub>3</sub>Ni(111) with Pt overlayer is not only high efficient for ORR reaction at the cathode of PEMFCs but also highly active and selective for CO PROX in excess hydrogen. For Pt<sub>2</sub>Ni<sub>2</sub> and PtNi<sub>3</sub> surfaces, although the elementary oxidation reactions are very active, dramatic weak bonding between adsorbates and substrates and lower oxidation barriers for both oxidation reactions lead to poor overall reactivity and selectivity.

## ACKNOWLEDGMENTS

The present work is financially support by CAS “Bairen Project,” NSFC (Nos. 20503030 and 20733008), and MOST (No. 2007CB815205). We thank fruitful discussions with Qiang Fu and Ding Ma.

- <sup>1</sup>H. A. Gasteiger, N. Markovic, P. N. Ross, and J. E. Cairns, *J. Phys. Chem.* **98**, 617 (1994).
- <sup>2</sup>M. Watanabe, H. Igarashi, and T. Fujino, *Electrochemistry (Tokyo, Jpn.)* **67**, 1194 (1999).
- <sup>3</sup>G. Avgouropoulos and T. Ioannides, *Appl. Catal., B* **56**, 77 (2005).
- <sup>4</sup>K. Wang, H. A. Gasteiger, N. M. Markovic, and P. N. Ross, *Electrochim. Acta* **41**, 2587 (1996).
- <sup>5</sup>C. Dupont, Y. Jugnet, and D. Loffreda, *J. Am. Chem. Soc.* **128**, 9129 (2006).
- <sup>6</sup>S. Mukerjee and S. Srinivasan, *J. Electroanal. Chem.* **357**, 201 (1993).
- <sup>7</sup>J. Zhang, M. B. Vukmirovic, K. Sasaki, A. U. Nilekar, M. Mavrikakis, and R. R. Adzic, *J. Am. Chem. Soc.* **127**, 12480 (2005).
- <sup>8</sup>J. Zhang, M. B. Vukmirovic, Y. Xu, M. Mavrikakis, and R. R. Adzic, *Angew. Chem., Int. Ed.* **44**, 2132 (2005).
- <sup>9</sup>D. A. Stevens, J. M. Rouleau, R. E. Mar, A. Bonakdarpour, R. T. Atanasoski, A. K. Schmoekkel, M. K. Debe, and J. R. Dahna, *J. Electrochem. Soc.* **154**, B556 (2007).
- <sup>10</sup>V. R. Stamenkovic, B. S. Mun, M. Arenz, K. J. J. Mayrhofer, C. A. Lucas, G. Wang, P. N. Ross, and N. M. Markovic, *Nat. Mater.* **6**, 241 (2007). V. R. Stamenkovic, B. Flower, B. S. Mun, G. Wang, P. N. Ross, C. A. Lucas, and N. M. Markovic, *Science* **315**, 493 (2007).
- <sup>11</sup>V. R. Stamenkovic, B. S. Mun, K. J. J. Mayrhofer, P. N. Ross, N. M. Markovic, J. Rossmeisl, J. Greeley, and J. K. Nørskov, *Angew. Chem., Int. Ed.* **45**, 2897 (2006).
- <sup>12</sup>E. Christoffersen, P. Liu, A. Ruban, H. L. Skriver, and J. K. Nørskov, *J. Catal.* **199**, 123 (2001).
- <sup>13</sup>J. Greeley and M. Mavrikakis, *Nat. Mater.* **3**, 810 (2004).
- <sup>14</sup>J. Greeley, T. F. Jaramillo, J. Bonde, I. Chorkendorff, and J. K. Nørskov, *Nat. Mater.* **5**, 909 (2006).
- <sup>15</sup>E. Santos and W. Schmickler, *Angew. Chem., Int. Ed.* **46**, 8262 (2007).
- <sup>16</sup>M. M. Schubert, M. J. Kahlich, G. Feldmeyer, M. Huttner, S. Hackenberg, H. A. Gasteiger, and R. J. Behm, *Phys. Chem. Chem. Phys.* **3**, 1123 (2001).
- <sup>17</sup>A. Sirijaruphan, J. G. Goodwin, and R. W. Rice, *J. Catal.* **224**, 304 (2004).
- <sup>18</sup>P. Naknam, A. Luengnaruemitchai, S. Wongkasemjit, and S. Osuwan, *J. Power Sources* **165**, 353 (2007).
- <sup>19</sup>L. M. Chen, D. Ma, and X. H. Bao, *J. Phys. Chem. C* **111**, 2229 (2007).
- <sup>20</sup>V. R. Stamenkovic, M. Arenz, C. A. Lucas, M. E. Gallagher, P. N. Ross, and N. M. Markovic, *J. Am. Chem. Soc.* **125**, 2736 (2003).
- <sup>21</sup>V. Stamenkovic, M. Arenz, B. B. Bliznac, K. J. J. Mayrhofer, P. N. Ross, and N. M. Markovic, *Surf. Sci.* **576**, 145 (2005).
- <sup>22</sup>E. Y. Ko, E. D. Park, H. C. Lee, D. Lee, and S. Kim, *Angew. Chem., Int. Ed.* **46**, 734 (2007). E. Y. Ko, E. D. Park, K. W. Seo, H. C. Lee, D. Lee,

- and S. Kim, *Catal. Lett.* **110**, 275 (2006).
- <sup>23</sup> B. Hammer, L. B. Hansen, and J. K. Nørskov, *Phys. Rev. B* **59**, 7413 (1999).
- <sup>24</sup> J. P. Perdew, J. A. Chevary, S. H. Vosko, K. A. Jackson, M. R. Pederson, D. J. Singh, and C. Fiolhais, *Phys. Rev. B* **46**, 6671 (1992). J. A. White and D. M. Bird, *ibid.* **50**, 4954 (1994).
- <sup>25</sup> J. Neugebauer and M. Scheffler, *Phys. Rev. B* **46**, 16067 (1992).
- <sup>26</sup> T. Jacob and W. A. Goddard, *J. Phys. Chem. B* **108**, 8311 (2004).
- <sup>27</sup> S. Y. Choi, Y. S. Kwon, T. H. Rho, S. C. Hong, and J. I. Lee, *J. Korean Phys. Soc.* **37**, 104 (2000).
- <sup>28</sup> Y. Xu, A. V. Ruban, and M. Mavrikakis, *J. Am. Chem. Soc.* **126**, 4717 (2004).
- <sup>29</sup> NIST Computational Chemistry Comparison and Benchmark Database, NIST Standard Reference Database No. 101, Release 10 ed.; edited by R. D. Johnson III, 2004.
- <sup>30</sup> P. D. Nolan, B. R. Lutz, P. L. Tanaka, J. E. Davis, and C. B. Mullins, *J. Chem. Phys.* **111**, 3696 (1999).
- <sup>31</sup> Q. Liang, J. Yu, and J. Li, *J. Chem. Phys.* **125**, 054701 (2006).
- <sup>32</sup> D. C. Ford, Y. Xu, and M. Mavrikakis, *Surf. Sci.* **587**, 159 (2005).
- <sup>33</sup> J. L. Gland, B. A. Sexton, and G. B. Fisher, *Surf. Sci.* **95**, 587 (1980).
- <sup>34</sup> B. Poelsema, G. Mechttersheimer, and G. Comsa, *Surf. Sci.* **111**, 519 (1981).
- <sup>35</sup> Y. Y. Yeo, L. Vattuone, and D. A. King, *J. Chem. Phys.* **106**, 392 (1997).
- <sup>36</sup> X. Q. Gong, Z. P. Liu, R. Raval, and P. Hu, *J. Am. Chem. Soc.* **126**, 8 (2004).
- <sup>37</sup> S. Kandoi, A. A. Gokhale, L. C. Grabow, J. A. Dumesic, and M. Mavrikakis, *Catal. Lett.* **93**, 93 (2004).
- <sup>38</sup> J. Knudsen, A. U. Nilekar, R. T. Vang, J. Schnadt, E. L. Kunkes, J. A. Dumesic, M. Mavrikakis, and F. Besenbacher, *J. Am. Chem. Soc.* **129**, 6485 (2007).
- <sup>39</sup> L. E. Murillo, A. M. Goda, and J. G. Chen, *J. Am. Chem. Soc.* **129**, 7101 (2007).
- <sup>40</sup> J. R. Kitchin, J. K. Nørskov, M. A. Barteau, and J. G. Chen, *J. Chem. Phys.* **120**, 10240 (2004).
- <sup>41</sup> C. A. Menning, H. H. Hwu, and J. G. Chen, *J. Phys. Chem. B* **110**, 15471 (2006).
- <sup>42</sup> B. Hammer and J. K. Nørskov, *Surf. Sci.* **343**, 211 (1995).
- <sup>43</sup> J. K. Nørskov, T. Bligaard, A. Logadottir, S. Bahn, L. B. Hansen, M. Bollinger, H. Bengaard, B. Hammer, Z. Sljivancanin, M. Mavrikakis, Y. Xu, S. Dahl, and C. J. H. Jacobsen, *J. Catal.* **209**, 275 (2002).
- <sup>44</sup> Z. P. Liu and P. J. Hu, *J. Chem. Phys.* **115**, 4977 (2001).